UNIVERSITY OF CALIFORNIA,

IRVINE

Mechanical Investigation of a Novel Bio-Mimetic Morphing Structure

THESIS

submitted in partial satisfaction of the requirements

for the degree of

MASTER OF SCIENCE

In Materials Science and Engineering

by

Eva Maria Carreira Ramos

Thesis Committee:

Professor Lorenzo Valdevit, Chair

Professor Daniel R. Mumm

Professor Farghalli A. Mohamed

2009

The thesis of Eva Maria Carreira Ramos is approved:

_____

_____

_____

Committee Chair

University of California, Irvine

2009

TABLE OF CONTENTS

LIST OF FIGURES

ACKNOWLEDGMENTS

I would like to express the deepest gratitude and appreciation to my committee chair, Professor Lorenzo Valdevit for his guidance and persistent support.

I acknowledge the members of my committee: Professor Daniel Mumm and Professor Farghalli A. Mohamed.

In addition, I would like to thank all the members in my group and Professor Roger Rangel's group for the good work environment created and especially, to Anna Torrents who has always supported me.Gràcies Anna!

Finally, I would like to acknowledge the financial support from Balsells-Generalitat de Catalunya fellowship 2007-2008.

ABSTRACT OF THE THESIS

Mechanical Investigation of a Novel Bio-Mimetic Morphing Structure

By

Eva Maria Carreira Ramos

Master of Science in Materials Science and Engineering

University of California, Irvine, 2009

Professor Lorenzo Valdevit, Chair

This thesis presents a new approach to the design of biomimetic morphing structures: the inspiration comes from the exceptional characteristics of manta rays. Manta rays can weigh as much as 3.000 pounds and have a wing span in excess of 20 feet, and yet be incredibly agile: maneuvers resulting in 4-5 gs accelerations are not uncommon. The main morphological features of actual manta rays were recently studied and published in the literature. Based on those results, a synthetic prototype of a morphing wing is conceived and built. The structure comprises three main repeating elements: rigid platelets (bones), and two varieties of compliant connectors (cartilage). These three features result in a periodic planar structure that can be morphed with a combination of bending and twisting, thus mimicking an actual deformable swimming body. We suggest that this interesting deformed shape can be achieved with a reduced number of external actuators compared to competing concepts. The mechanical performance of the proposed structure upon actuation is investigated via a series of numerical simulations (based on

the commercial Finite Element package ABAQUS). Although extensive amount of work in this project is still underway (mostly regarding manufacturability, actuation schemes and durability), this work supports a novel approach for the design of high-authority morphing structures.

1. INTRODUCTION

Nowadays, maneuverable underwater vehicles are affected by deficiencies due to the use of traditional propulsive techniques, i.e. rotary motors and their related difficulty and expensive repairs. Attempts to build faster and more efficient vehicles have been made in the biomimetic morphing structures field.

The manta ray and other batoid fishes are an excellent inspiration for autonomous underwater vehicles due to being extremely efficient swimmers, propulsing in some cases as much as 5.000 lb of weight and 25 ft across length body. Moreover, they can cruise at high speeds and can perform 4-5 gs acceleration when maneuvering. Due to all these properties, the efforts have been focused in the design of a morphing plate with these characteristics: low actuation energy, high authority, ability to morph into complex shapes, and large stroke. Two different approaches have excelled in achieving many of these characteristics: corrugated core sandwich beams and kagome based sandwich plates [9-18]. One last approach is the use of tensegrity structures to mimic the locomotion of these fishes [19-21].

In this paper, a different approach to the structural foundation of the bio-inspired morphing wing is used, based on the last studies of the morphology of the actual manta ray [1-8]. Radials are the basis of locomotion of batoid fish; a unit cell based on interradial joints (cross-bracing) is detected in oscillatory swimmers [1]. A synthetic prototype is conceived and built based on three main repeating elements: rigid platelets (bones), and two varieties of compliant connectors (cartilage). These three features result in a periodic planar structure that can be morphed with a combination of bending and

twisting so, mimicking an actual deformable swimming body. The mechanical performance of such structure upon actuation is investigated through numerical simulations (based on the commercial Finite Element package ABAQUS). Additionaly, different types of connectors are studied to gain a better understanding of the kinematic behavior of the morphing plate built and the deflections achieved are compared with those found in the references.

2. MORPHOLOGICAL FEATURES OF BATOID FISH

The exceptional swimming performance of several families of fish (in particular batoid fish) has motivated intense investigation into optimal design principles for bio-mimetic morphing structures [9-21]. Mimicking the undulation of fish tails and wings has been the focus of most of the activity in this area. Although some performance metrics of batoid fish were demonstrated with synthetic structures [19, 21], the synthetic structure design is based on standard mechanical engineering concepts (trusses, frames, tensegrity structures). To the best of our knowledge, very few attempts have been made to identify the morphological features that enable batoid fish's phenomenal performance metrics and reproduce them in a synthetic structure. This was partly due to the lack of information about the morphology of these animals. A series of very careful biological and biomechanical studies of various families of manta rays have been published [1-8]. Based on these findings, our work focuses on mimicking the morphological features of the propulsion mechanism used by the manta ray uses to swim long distances at high speeds.

The main morphological features of batoid fish are presented in [1].

The pectoral fins of batoid fishes (stingrays, skates, sawfishes and guitarfishes) are long and fused to the cranium, forming in many cases large wing-like structures. These pectoral fins are usually used as the primary locomotion propulsors [3-4].

The skeleton of these "wings" for skates and rays is formed by a series of radially oriented cartilaginous fin rays whose origin is a modified pectoral girdle (the set of bones that connect the axial skeleton on each side) shown in Figure 1. Those fin rays are a

sequence of small and laterally oriented skeletal elements, radials that normally are represented by simple cylindrical building blocks.

Figure 1. Left, dorsal view of left side of the animal showing the pectoral girdle and the radials [1]. Right, Atlantic manta ray. [2].

Although some morphologic characteristics are common for all families of rays, the locomotion strategy can be very different. The swimming strategy is defined by the number of waves (f) moving across the wing during steady swimming. There are two extremes in the classification of rays according to their swimming strategy: oscillators and undulators. Oscillators flap the wings while maintaining $f<0.5$ at any given time [4]. Undulators often exhibit many waves moving along the wing ($f>1$). The majority of batoid fishes fall on a continuum from undulatory to oscillatory locomotion, that is, their kinematic motion falls between these extremes.

The wing skeleton that allows these waves to be propagated consists, as mentioned before, of an array of serially repeating cartilaginous elements that start in the pectoral girdle and consist of many long, tapering fin rays [5] that bifurcate once or twice before

reaching the edge of the wing. Each fin ray is composed of cylindrical skeletal elements, radials, stacked end-to-end, much like carpals.

In oscillatory swimmers there is an interconnection between these fin rays in the central areas of the wing that undulatory swimmers do not show. These morphological variations are attributed to the need of having different areas of the wing stiffened of oscillatory swimmers compared to undulatory ones.

The actuation of this skeleton is done by long thin muscles that run from the craniocaudally expanded pectoral girdle along each of the fin rays, inserting on every radial [6]. During locomotion, the radials are flexed dorsally by dorsal adductor muscles and ventrally flexed by less massive ventral abductors. Although the relative rotation of two adjacent radials in a fin ray is small (~15 degrees) [7], there are enough radials, and therefore interradial joints, that the wingtips of rapidly swimming oscillatory rays often touch behind their back [8]. A morphological trade-off is evident: the interradial joints must be mobile to provide flexibility to the wing, yet the radials must be stiff enough to transmit the force of the wing musculature.

In [1], the pattern of mineralization in the wing skeleton of 12 families of batoid fishes was thoroughly investigated at several scales: (i) fine or small scale (calcification patterns), (ii) medium scale (shape and structure of individual radials) and, (iii) large scale (arrangement of radials).

The research done regarding the individual radials is basic for the present work because, as stated before, radials play a fundamental role in the motion of rays.

For all the families studied, the cross-section of radials varies within and among the species and this cross-sectional shape changes with position on the wing depending on the individuals. In addition, some species exhibit interradial connections –cross-braces; each cross brace connects two radials in adjacent fin rays in some areas of the wing (Figure 2). Cross-bracing is observed in medial areas of the wing of semi-oscillatory and oscillatory swimmers (Figure 3) occupying, in some cases, the major part of the wing.

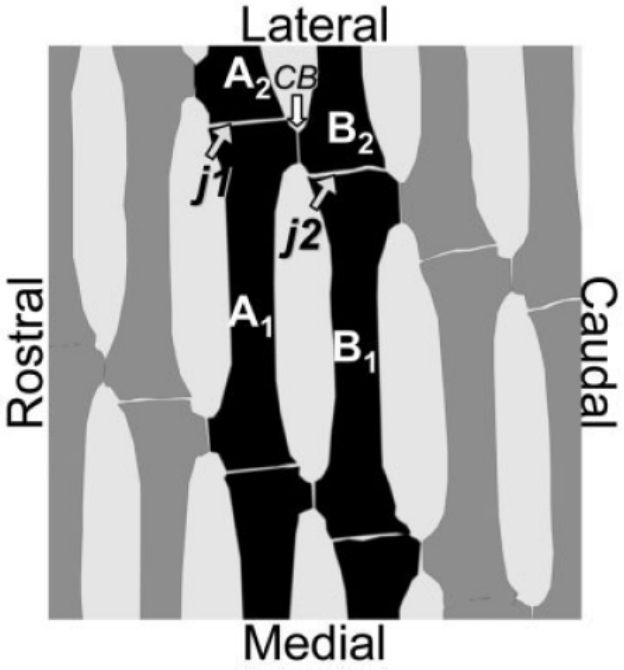

Figure 2. Schematic of cross-bracing. Fin ray “A” is joined to fin ray “B” by a cartilaginous extension (CB). This inhibits the bending of normal radial joints j1 and j2. Radial A1 will bend when the joint between radials B1 and B2 tries to bend. J2 loses the ability to bend in this motion. These cross-braces are arranged in diagonal patterns such that the entire area is reinforced and stiffened. [1]

Cross-braces occur contralaterally and at opposite ends of the radial, where the proximal brace is placed on the anterior side. The fact that these connections are repeated through the area where cross-bracing occurs and are found in both sides of the animal (among other things), gives these oscillatory swimmers potential for side-specific effects on locomotion.

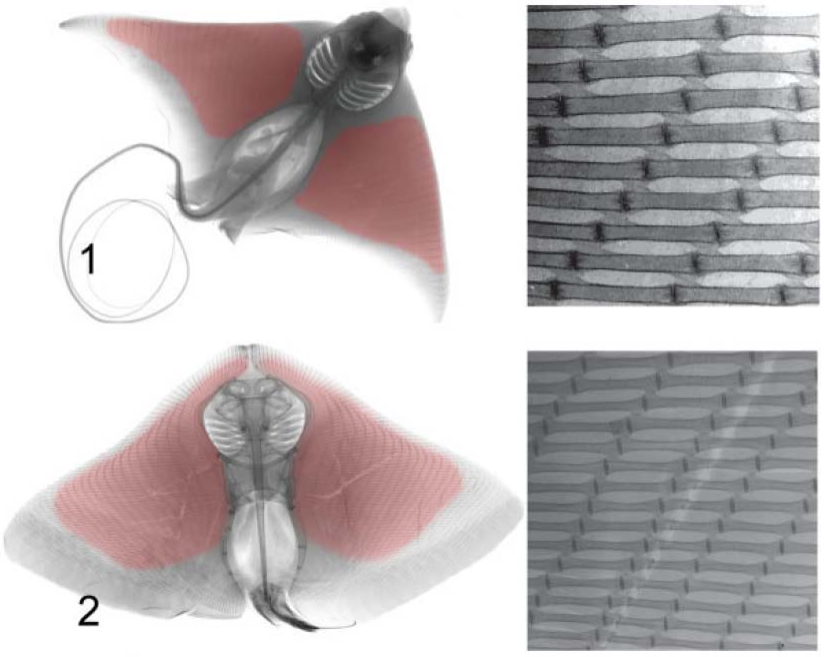

Figure 3. Cross bracing in oscillatory swimmers. The red zones on the wings of the different family specimens indicate the areas in which cross-bracing is found. Magnified images of the wing appear next to the species and demonstrate variations in the cross-bracing found in many species of oscillatory swimmers. Figures not to scale. [1]

The projected shape and the length of the radials, although generally rectangular in shape, vary among species [1].

Mimicking locomotion of oscillatory swimmers following the cross-bracing pattern (Figure 2) in a synthetic planar structure, could present advantages compared to competing concepts presented in the next chapter.

3. SYNTHETIC MORPHING STRUCTURES

The approaches to build fast, efficient, and maneuverable underwater vehicles have looked to nature for inspiration.

Traditional propulsive techniques have been based on rotary motors. The disadvantages of these methods are the imperfect sealing, low efficiency, low engine life and difficult repairs when needed.

Several attempts have been made to overcome the limitations of the traditional propulsion methods [9-21].

The unifying theme has been the quest to design a morphing plate (or shell) with the following characteristics: (i) low actuation energy; (ii) high-authority (i.e. the ability to actuate against restraining loads); (iii) ability to morph into complex shapes; (iv) large stroke. Two structures that excel in (i-iii) are the corrugated-core sandwich beam (in 1D) [9-17] and the kagome-based sandwich plate (in 3D) [18].

3.1 Corrugated-core Sandwich Beam

An implementation of the corrugated-core sandwich concept is depicted in Figure 4. A selected number of face members (potentially one entire face) can be replaced by linear actuators. Upon contraction of the actuators, the entire beam bends as a whole. In the

limit in which the members are pin jointed (obviously an idealization), each member only experiences axial stress, resulting in a stretching-dominated structure. The implication is that such a structure is capable of achieving a large fraction of the zero load stroke even when actuation is resisted by external forces.

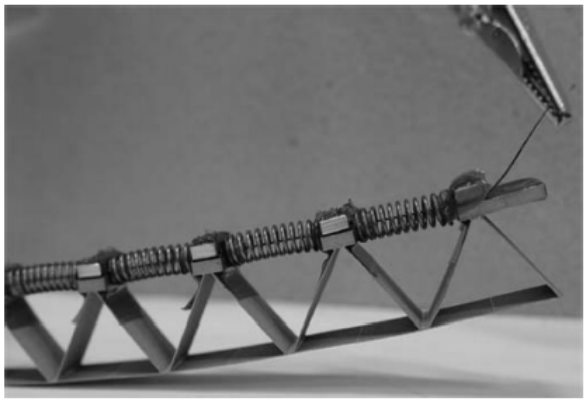

(a)

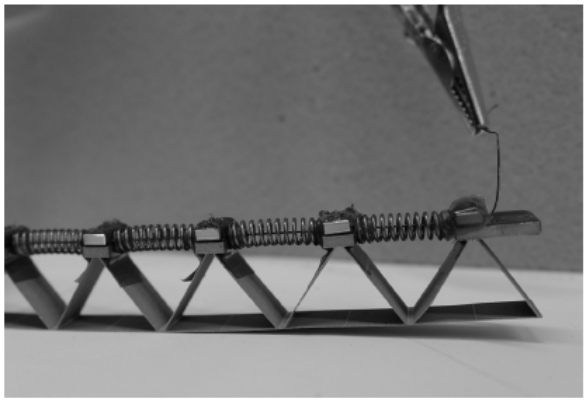

(b)

Figure 4. An optimal SMA actuator: (a) activated position; (b) recovered position [11]

SMAs exhibit large inelastic recoverable deformation (several percent), large actuation stress (hundreds of MPa) and simple actuation mechanism (resistive heating) [9-10]. Additionally, they don’t require large available volume.

Pre-stretched, one-way SMA linear actuators contract upon heating above a critical (austenite start) temperature. However, in the absence of an applied tensile load, these actuators do not ‘re-stretch’ upon cooling [10]. The design of a two-way morphing structure with a one-way SMA actuator requires some ingenuity. One solution envisions the insertion of elastic springs in parallel with the morphing elements (Figure 4). Upon cooling, the SMA transforms back to its martensitic phase (characterized by a low yield strength) and is permanently stretched to its initial configuration by the action of the springs. An alternative solution combines two corrugated core sandwiches, joined by a passive (shear resistant) face sheet and each with the active face on the outside [13-16]. When one active face is heated up, it will contract yielding the opposite face (martensitic) in tension. Upon cooling of the first face (and its transformation to martensitic phase), and heating of the second active face, this latter face will contract and stretch the first face in tension. This cyclic behavior results in two-way operation. The design was later improved modifying the core topology and the shape memory pre-strain [14]. Lastly, the core has been replaced with a structure that used freely rotating, revolute joints between the unit cells [15], which reduced the elastic energy stored in the core. Each of these devices consisted of a series of linearly repeating antagonistic flexural unit cells (AFC) [16] shown in Figure 5.

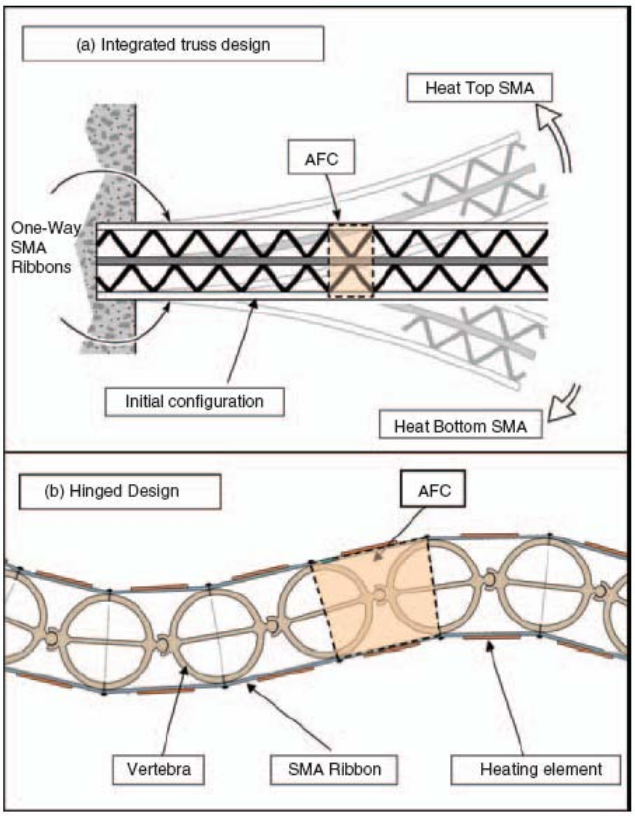

Figure 5. (a) A cantilever sandwich beam constructed from a triangular corrugated core and pre-strained shape memory alloy face sheets. Heating one side causes contraction of that face sheet, and consequent tensile elongation of the non-heated face sheet, and an overall flexural deformation of the beam and (b) alternative design in which the core facilitates bending between the adjacent unit cells via rotation joints (vertebra) [16].

It should be briefly mentioned that two-way SMAs do exist, but they require extensive training and their performance (particularly in fatigue) is not nearly as desirable relative to one-way SMAs.

The corrugated-core structure enables actuation in one direction only. If more complex shapes are desired (e.g. combined twisting and bending), 3D concepts need to be explored.

3.2 Kagome-based Sandwich Plate

Guest and Hutchinson showed that no infinite truss can be simultaneously statically determinate and stiff [17]. An exception exists for finite structures: it consists of two truss face sheets with a kagome pattern (a combination of hexagons and triangles) sandwiched by a tetrahedral truss core. One truss face can be replaced by a thin stiffness-matched continuous face without excessive detriment in the properties. Such a structure was built and bending and twisting motion with high-authority performance successfully demonstrated [18].

The design consisted of an active back-plane comprising a Kagome truss, capable of changing the shape of a solid face, connected to the back plane by means of a tetrahedral truss core shown in Figure 6 [19]. A version of the structure was manufactured using stainless steel active face and core, with a polycarbonate passive face, and commercially available linear stepper actuators. Simple stepping motors were used as actuators (replacing some back-face truss members). It was shown that, while the structure is capable of sustaining large passive loads at low weight, the system is actuator-limited.

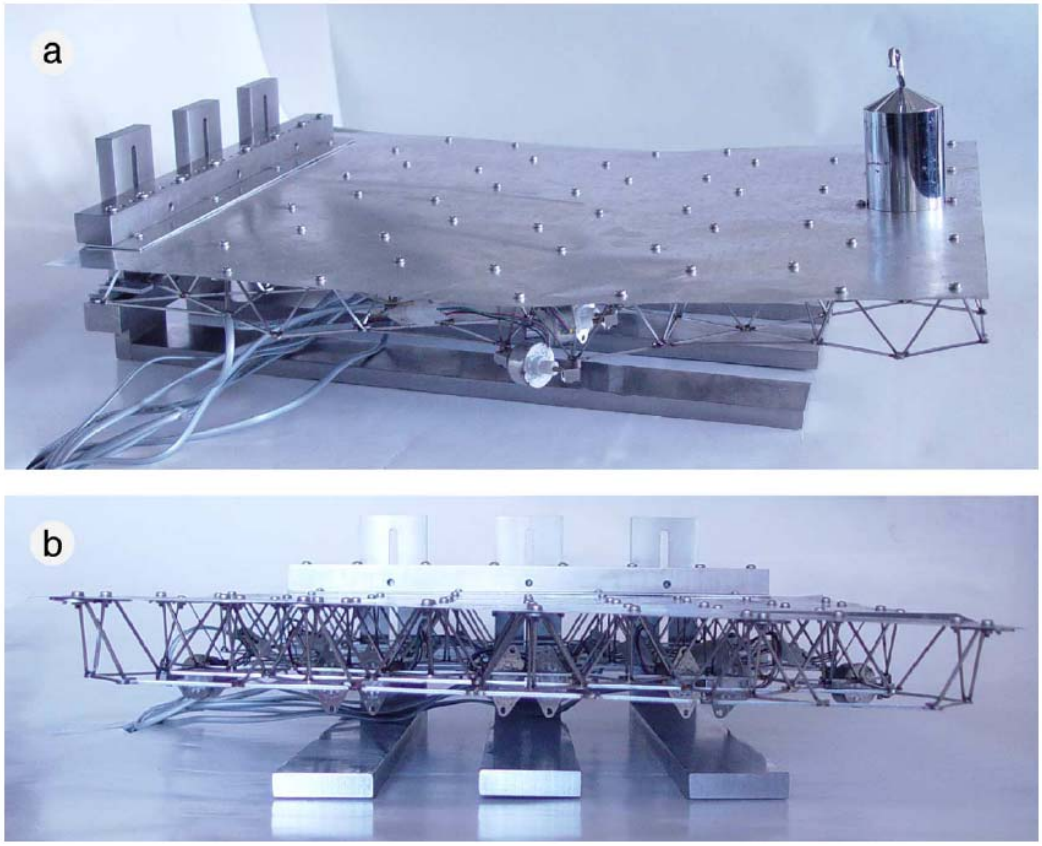

Figure 6. Hinging and twisting modes when an Al alloy face sheet is used [18].

Both the 1D and 2D structures defined above are very limited in the maximum achievable stroke. Ultimately, they are limited by the yield strain of the metal used.

3.3 Tensegrity-based Morphing Concepts

Recently, H. Bart-Smith and co-authors at the University of Virginia have conceived and designed a structure that overcomes this limitation. Their work is inspired by the performance of the manta ray and other batoid fish and aims at developing a structure that can propel an underwater vehicle with the swift and silent motions of the manta ray. To achieve this goal, she and her group have designed a lightweight control surface,

manipulated by an active tensegrity structure, with high out-of plane stiffness and a large range of motion under large restraining moments [20, 22].

Tensegrity structures are comprised of a set of discontinuous compressed struts held together with a continuous web of tensioned cables [21]. They offer high strength to mass ratios, low mechanical wear in dynamical applications, and high deformability with minimal input energy, which makes these systems excellent candidates for the structural layout of a morphing wing. In [20], the wing is actuated by replacing passive cables and struts with actuators.

The location and selected motion of each actuator was optimized with the goal of achieving a displacement field as close as possible to that of a cownose ray (no data were available for the manta ray).

Such a structure enables complex actuation shapes and previously unattainable displacements and rotations. On the other hand, robustness is a concern (breakage of one link in the structure can be disastrous). We also notice that tensegrity structures are substantially different from the morphology of a ray. Although they meet a bio-mimetic objective, they do not constitute a bio-mimetic design.

In the previous chapter, we present an alternative morphing structure based on the skeletal structure of some common rays (Figure 2-3). Such structure is capable of morphing into complex shapes (bending+twisting) at large stroke, and requires a limited number of actuators.

4. A novel biomimetic morphing concept: numerical study and prototype demonstration

The cross-braced portion of batoid fish wings (Figure 7a, see Chapter 2 and [1]) reveals an interesting structure from the point of view of shape change (morphing). Each individual bone platelet can be thought of a rigid component, connected to its nearest neighbors by means of flexible joints. Each joint can only flex a small amount (~15 degrees, for typical rays [7], but on the wing size scale, substantial flexure and twisting is achievable. We tried to capture this morphological feature in a synthetic structure. A detail of the prototype is depicted in Figure 7b.

The bone platelets are modeled with Aluminum bars with square cross-section, whereas the joints are Nylon 6-6 screws.

Each Aluminum bar was 1" long and had a square cross-section with a side of ¼". 63 bars were used. Side connectors are positioned at ¼" from the edge of the bar. These dimensions were chosen to maintain the aspect ratio for the radials described in Schaefer's paper [1], due to the unavailability of more detailed information. It's also important to remark that in the biological structure, the dimensions of the radials and joints depend on the position in the wing and on the fish family. This aspect was not reproduced in the synthetic prototype, which was chosen perfectly periodic.

The holes were drilled in the 63 bars with a Bridgeport CNC mill located in the Engineering Gateway machine shop. Each hole was tapped manually for the sake of the prototype realization. The hand process described above is responsible for the tolerances

observable in Figure 7b. More automatic and accurate manufacturing techniques are currently under investigation.

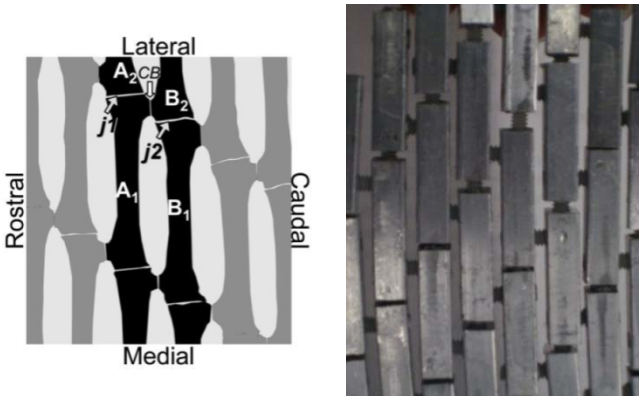

Figure 7. On the left, the cross bracing unit cell [1]. On the right, the actual structure.

Even with lower than desirable tolerances, an interesting kinematic mechanism was clearly observed (Figure 8).

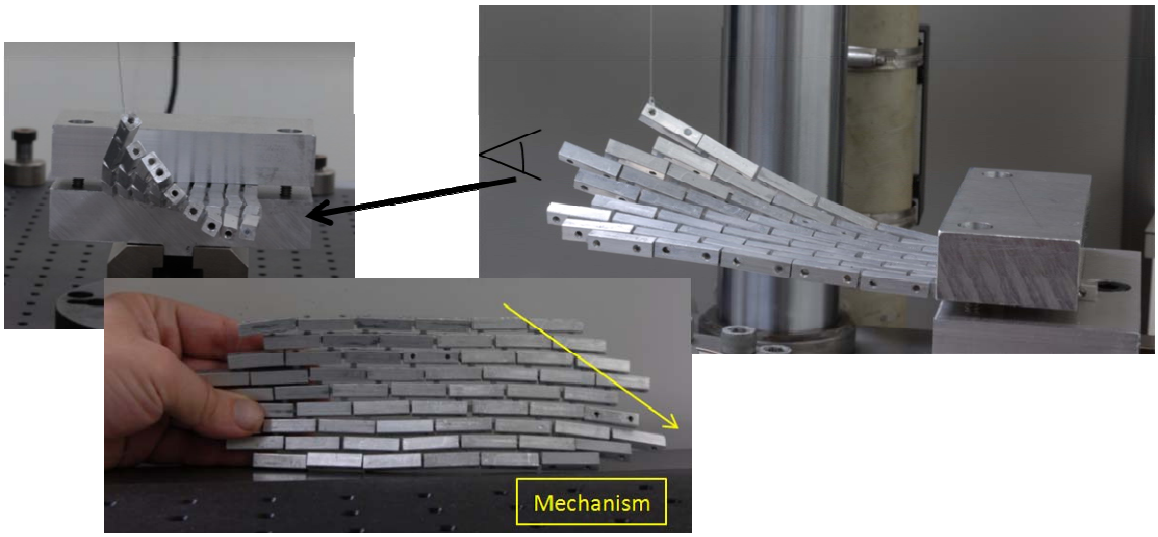

Figure 8. Mechanism when actuating the structure pulling up from one end.

This mechanism is oriented at 45 degrees from the horizontal in the structure of Figure 8 and 9. In other words, the structure is able to flex with virtually zero resistance along one diagonal, whereas a much stiffer behavior is expected along the perpendicular diagonal. Such mechanism allows interesting actuation patterns with a very limited number of actuators. Theoretically, one actuator (connected to the morphing plate by some truss structure on one side) should guarantee a swimming-like motion.

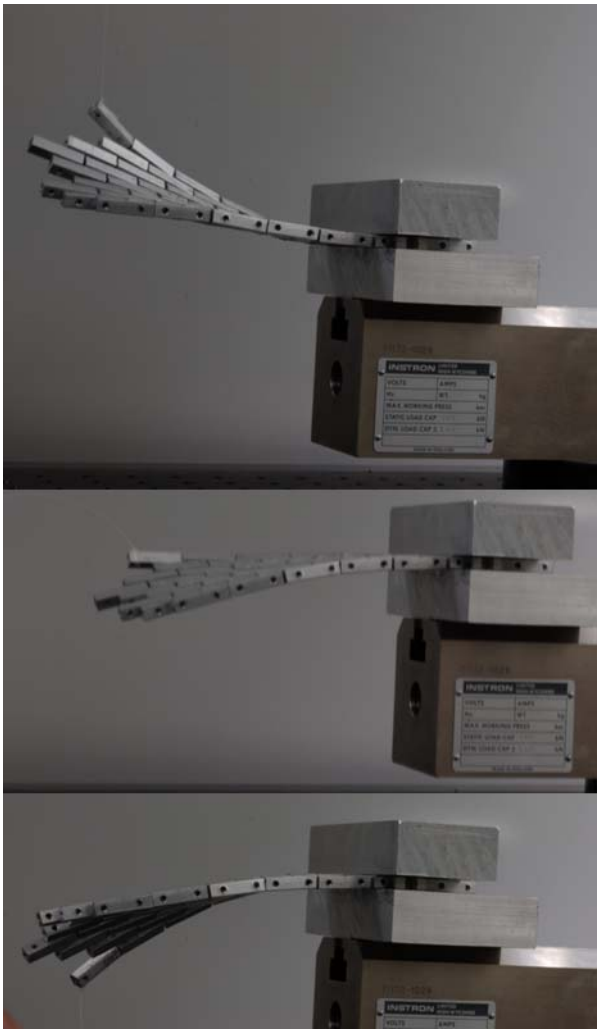

Figure 9. Swimming-like motion achieved by the prototype

This contrasts with the competing concepts presented in Chapter 3, for which several actuators are typically necessary to achieve interesting combinations of bending and twisting [18-20, 22].

In order to demonstrate the mechanical behavior of this morphing structure, a Finite Element model was built and simulated with the commercial code ABAQUS ©.

4.1 The Finite Element Model

Both the rigid bars and the connectors were modeled with beam elements. The bars are given a rectangular cross-section and assigned the properties of a typical high-strength Aluminum ($E = 70\,GPa;\ \nu = 0.3;\sigma_Y = 350\,MPa$ [23]). The connectors were modeled as beams with a generalized section, and assigned the properties of Nylon 6-6 ($E = 2.45\,GPa;\ \nu = 0.3;\mathsf{K}\ \sigma_Y = 100\,MPa$ [23]). The choice of a generalized section was motivated by the necessity to assign independently modifiable values for torsional and bending stiffness, to simulate various types of connectors and gain a better understanding of the kinematic behavior of the morphing plate. All the six degrees of freedom of the bars and the connectors were linked at the connection points using the *TIE keyword in ABAQUS [22].

The diameter of the connectors is 0.002 m (the same dimension as the screws in the prototype), resulting in a section area of 3.1416E-06 m^2.

For connectors with a circular cross-section, the moments of inertia along the x and y axes in the cross-section are $I_{11} = I_{22} = \frac{\pi \cdot R^4}{4} = 7.854E - 13\ m^4$. The cross-product of inertia I_{12} is obviously zero.

For a solid circular beam, the torsional modulus J is given by: $J = \frac{1}{2} \cdot \pi \cdot R^4$

In the prototype (or in a real system), the degree of torsional constraint at the node is not necessarily well represented by that corresponding to two welded beams. For example, in the case of the prototype (where screws are used to secure mechanical joining of bars and connectors), the screws offer substantial bending stiffness but virtually no torsional stiffness at the connections (if friction on the threads is neglected). To study the effect of the ratio of bending to torsional stiffness of the connectors –on the results, we ran two sets of simulations: (i) one in which the connectors are simply circular section beams welded to the bars (resulting in a torsional modulus of $J^{(i)} = 1.5708 \cdot 10^{-12}$ m^4, and (ii) one in which the torsional modulus is decreased by a factor 100 relative to case (i) (resulting in $J^{(ii)} = J^{(i)}/100 = 1.5708 \cdot 10^{-14}$ m^4).

Sectorial moment of the section (Gamma O) and warping constants are assumed to be equal to zero.

All six degrees of freedom were constrained for the nodes shown in Figure 10. A displacement of 0.4 m was applied to the node marked in purple (Node 2).

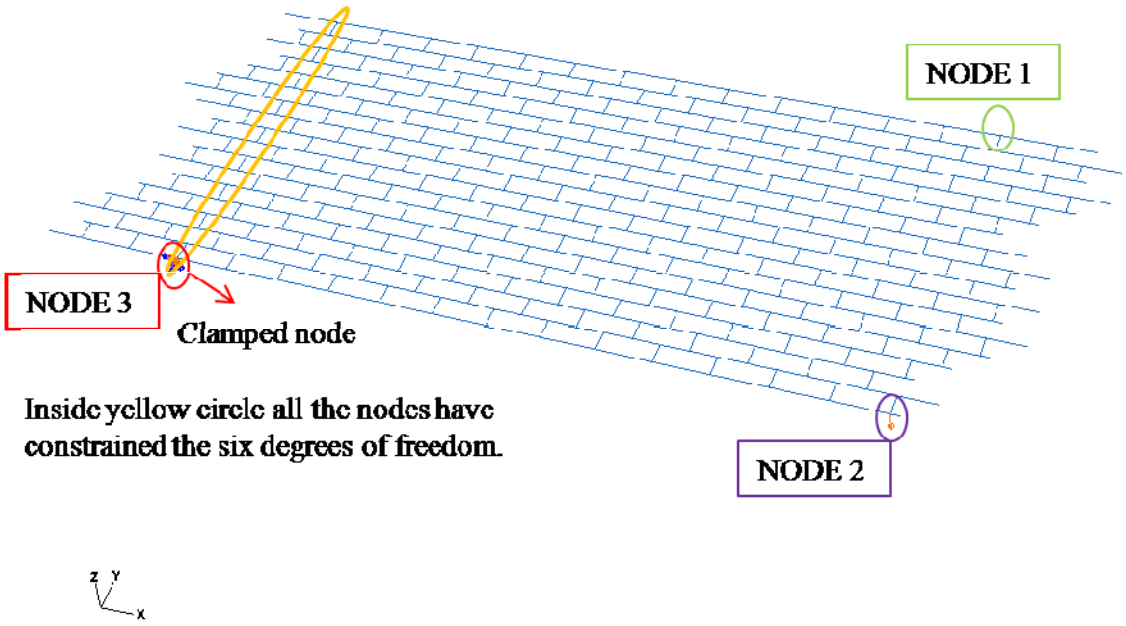

Figure 10. Representation of the boundary conditions and the studied nodes.

We define u_2 and u_1 as the component of the displacement in the out-of-plane (z) direction of node 2 and 1 respectively, where node 2 is the point at which the displacement is applied and node 1 has the same x-coordinate as node 2, but is located at the opposite side of the plate (see Figure 10).

A sequence of images is shown for the case where the torsional rigidity of the connector is that corresponding to a nylon bar with circular cross-section. The perspective is in the same as in Figure 10.

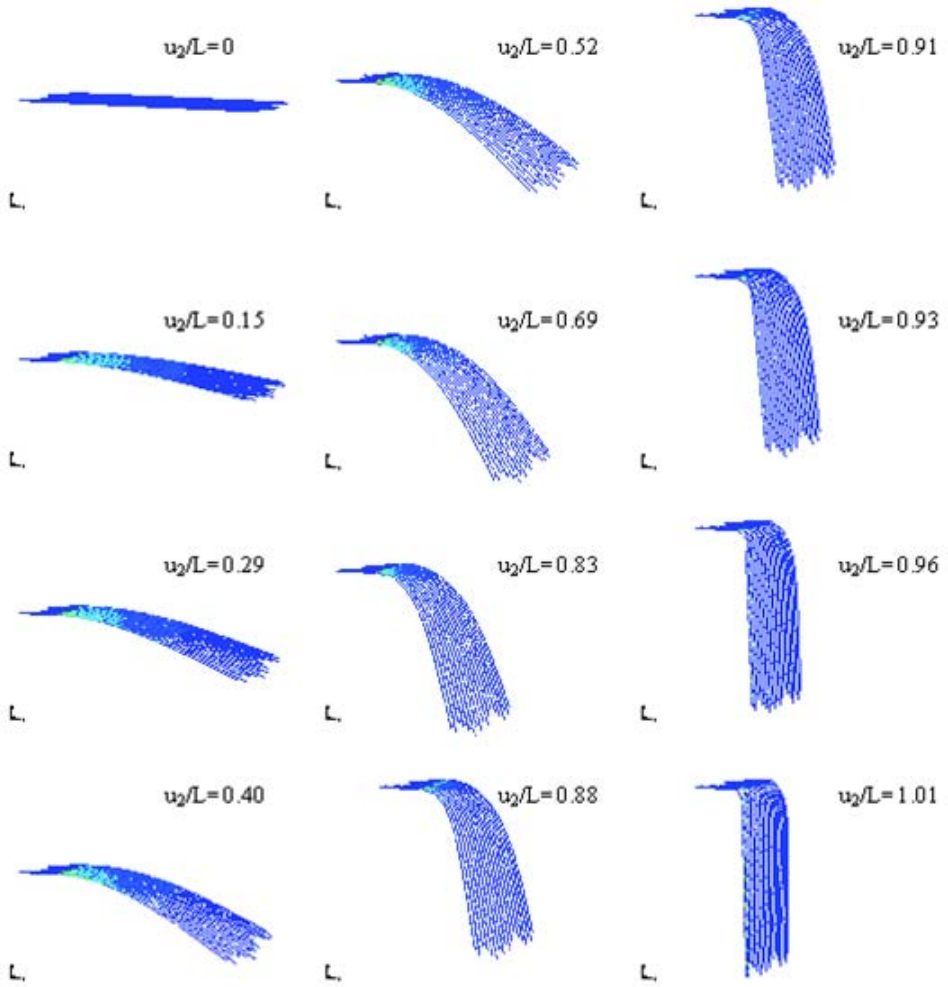

Figure 11. Images showing the motion of the model. The sequence can be seen down and right.

To analyze the results and compare the effect of the different torsional rigidity parameters, three plots will be shown for each simulation.

The first plot (Figure 12) represents the force needed to apply the imposed displacement: F as a function of u_2/L.

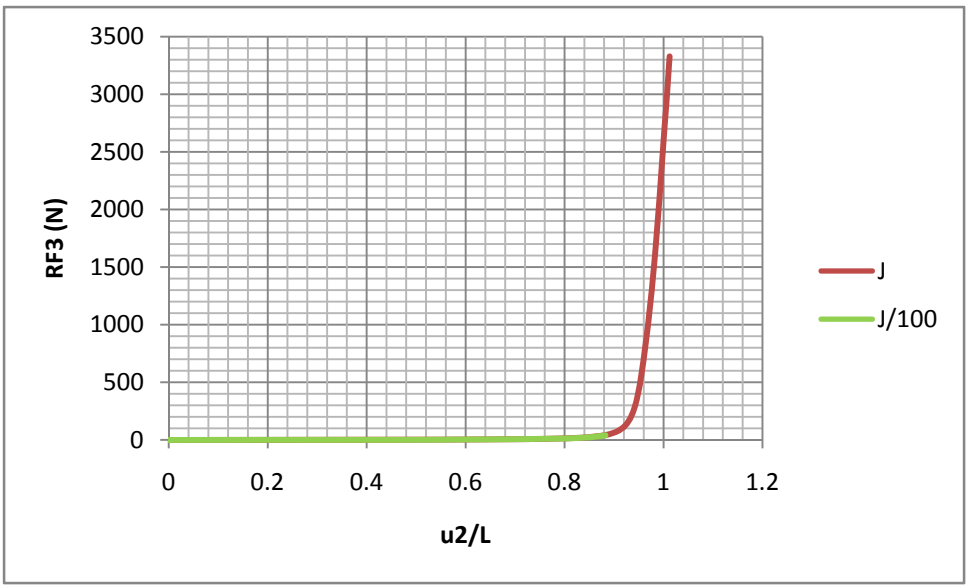

Figure 12. Force applied in node 3 in the z component as a function of normalized displacement in node 2. J/100 calculation stopped at 87% of the set up deformation.

As can be seen in the previous plot (Figure 12), the necessary force to pull down the structure is mostly linear until we reach the point where the structure blocks. That moment comes when the relation between the displacement of the node from which we are pulling (Node 2) and the length of the structure is 0.9.

When the torsional rigidity of the screws is lower (J/100), the calculation doesn't converge until the end. It can be seen that the overall behavior is the same for both calculations.

However, for the shown curves, more force for the calculation with more resistance to rotate was expected. Amplifying the first part of the previous graph:

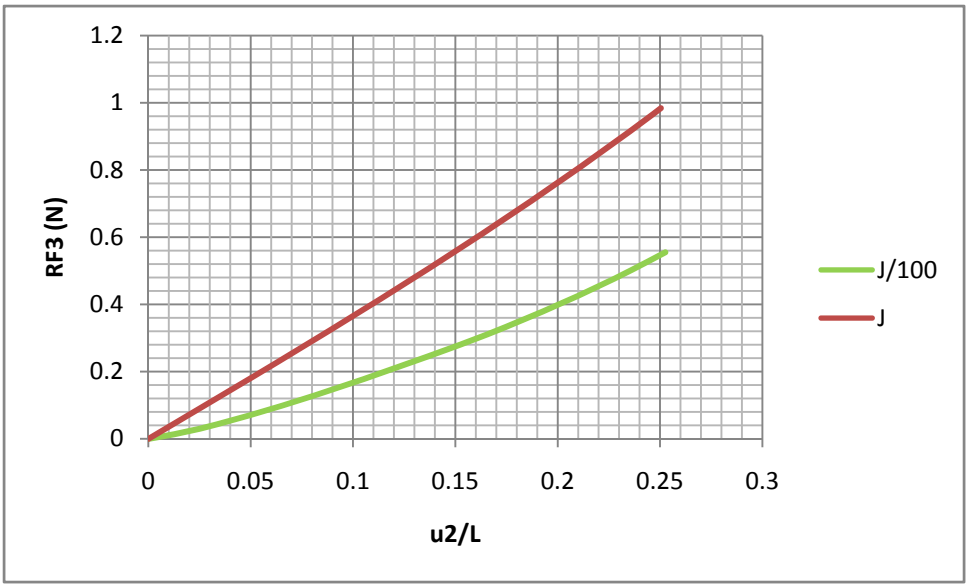

Figure 13. Force applied in node 3 in the z component as a function of normalized displacement in node 2. J/100 calculation stopped at 87% of the set up deformation. The scale has been reduced to 0.3 for the abscises axis

The predicted result is shown in Figure 13. The force required to pull down the structure to the same point is lower for the case in which the torsional rigidity is lower.

The second plot (Figure 14) represents the twist angle (measured as $\frac{u_2-u_1}{L}$) as a function of u_2/L. Here the twisting and bending processes can be evaluated.

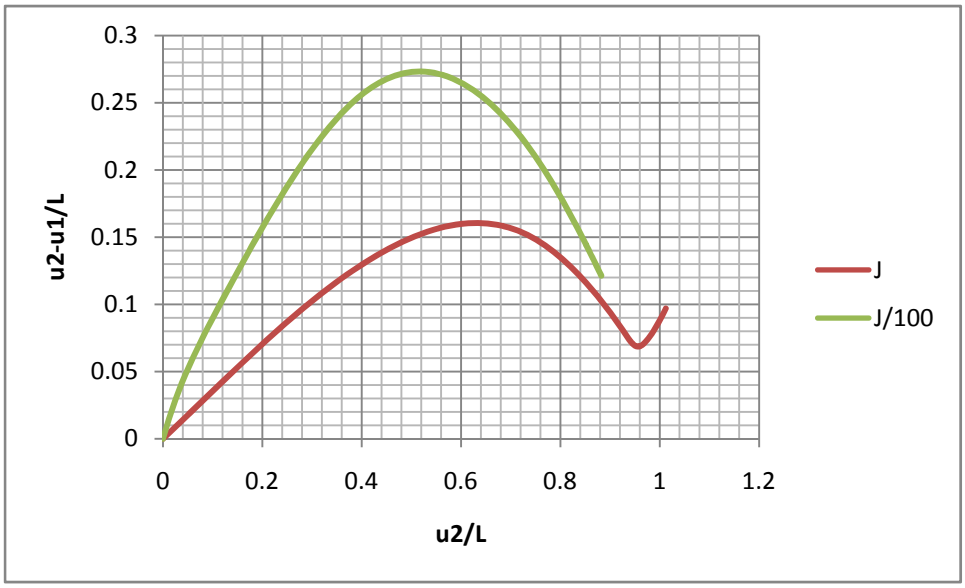

Figure 14. 'Angle' between node 1 and 2 as a function of normalized displacement in node 2. J/100 calculation stopped at 87% of the set up deformation.

Correlating what Figure 14 shows to what happens in the simulation summarized in Figure 11, it can be said that the structure undergoes different situations.

The first situation is given from the begining until the maximum point in the curves, (twisting of the structure) shown in Figure. 15. The node from which the structure is pulled down (u_2) is always in a lower position than the node in the other extreme in y direction (u_1).

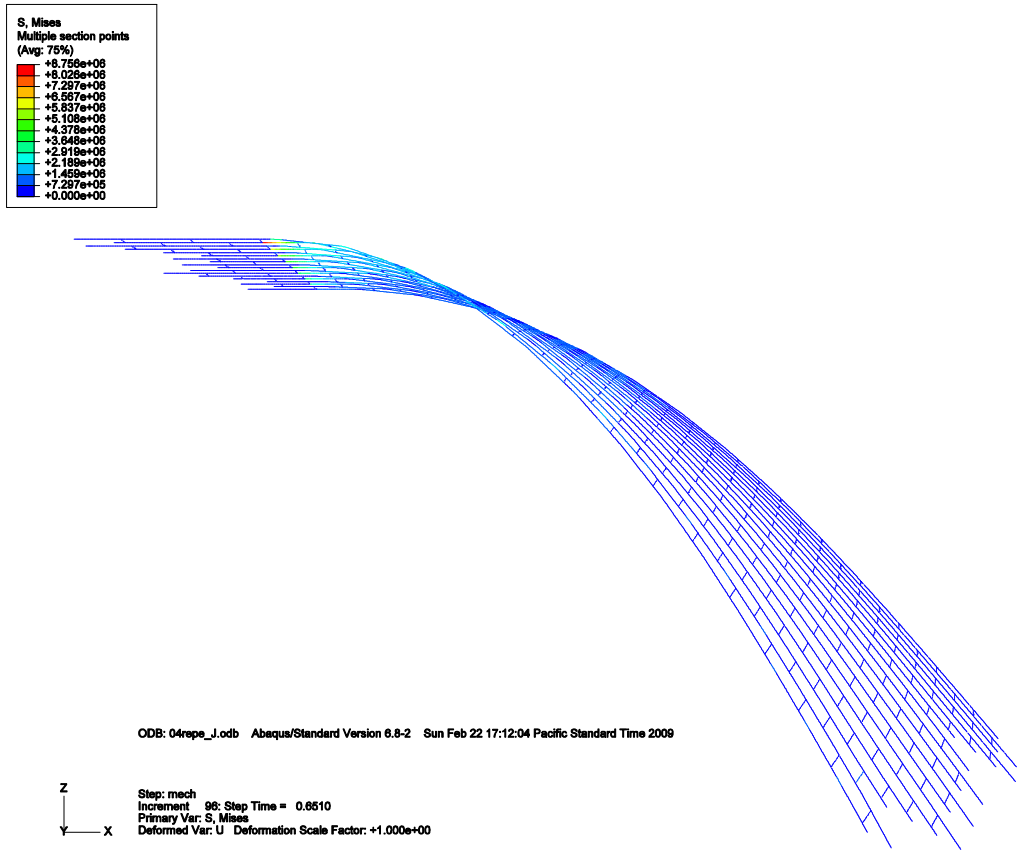

Figure 15. Maximum twisting produced in the motion of the wing.

The second situation comes when the structure cannot twist more because it is blocked. In this situation, the bending starts and both nodes go down. Here, due to the way the structure is actuated (linearly in –z direction) and the initial position from which the twisting phase starts, the u_1 is displaced down faster than u_2. Important to notice here, and once again that all the values represented are for the z component of the parameters.

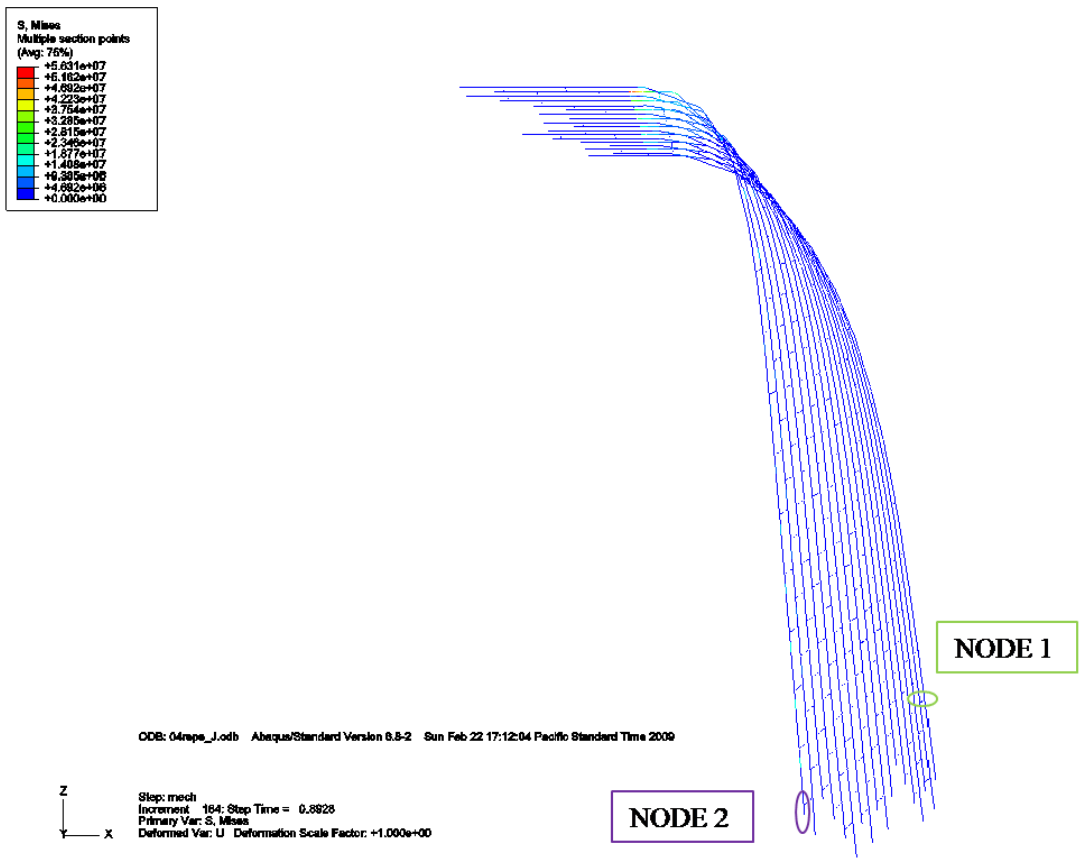

Figure 16. Final of the bending phase. Nodes 1 and 2 are closer than in the previous phase.

There would be another one that is only appreciated for the J simulation. In this third one, the structure is already pointing down to the –z direction and what we do is to deform the structure as if we were in a tensile test. That is why at this point, in the force representation, the force required to take down the node 2 increases drastically.

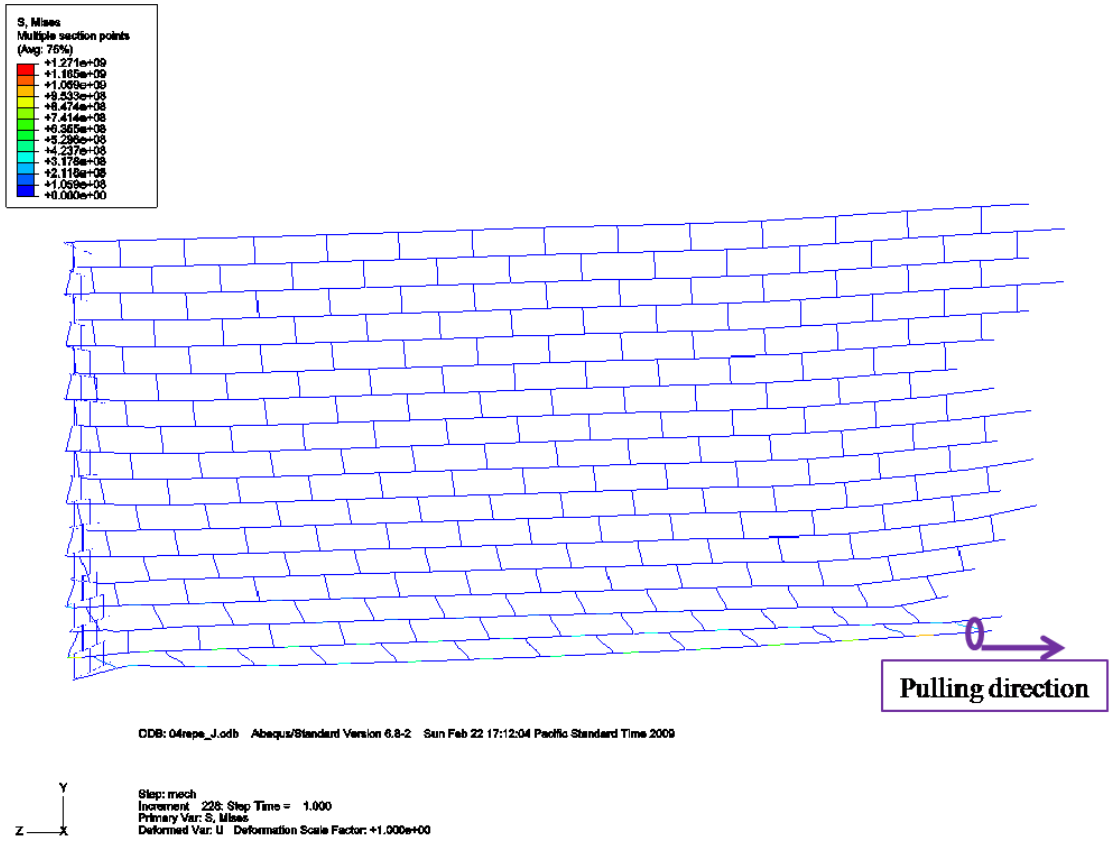

Figure 17. Final step of the simulation. The pulling direction and the node 2 are marked.

Additionally, it is noticeable that the structure with less torsional rigidity twists much more and gets blocked when the ratio u_2/L is lower.

The third plot (Figure 18) represents u_1/L as a function of u_2/L and will give information about the progression of twist as the structure is deformed in bending.

u_1/L vs. u_2/L are represented to prove that the maximum seen in Figure 14 coincides with the point where the structure doesn't twist anymore and bending starts .

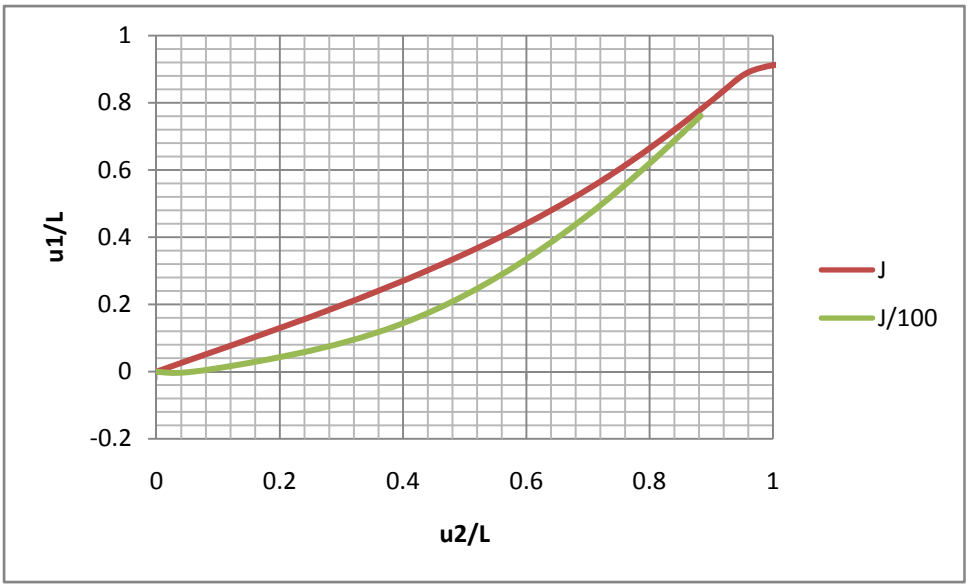

Figure 18. Component z of the displacement is represented for nodes 1 and 2 and for both simulations. J/100 calculation stopped at 87% of the set up deformation.

The change of slope can't be easily detected. However, the maximum angle shown in Graph 3. lays in the area where this change of slope is produced.

In the so called J calculation, the structure deforms 0.372 m (displacement of node 2 in –z axis) before the connectors fail (100 MPa).

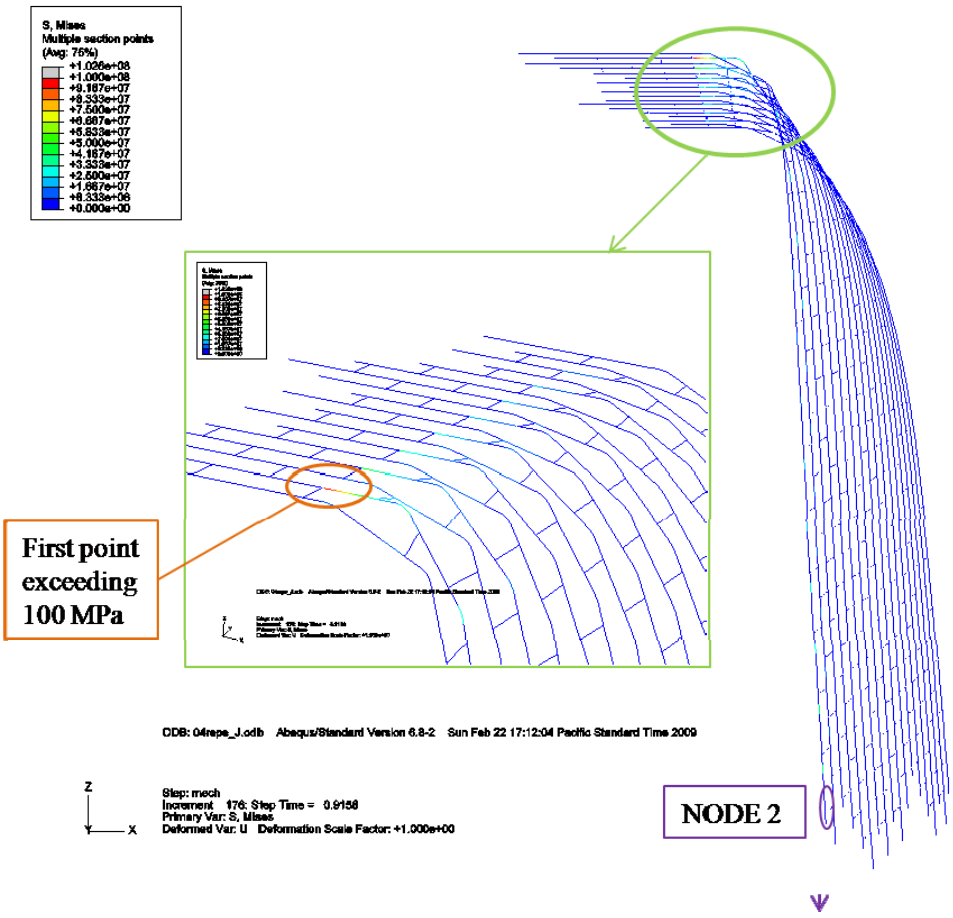

Figure 19. Failure point for the called 'J' calculation. The connector shown is the first point where the 100 MPa of the yielding stress are exceeded.

In the J/100 simulation, the structure deforms 0.348 m (displacement of node 2 in –z axis) before the calculation stops because it can't converge. Neither the bars nor the connectors fail while the structure reaches this deformation.

Once we have a good model for the simulations, representing quite acurately the way the structure behaves under the studied conditions, the next step would be to study the way our structure can be actuated.

Two possible options to actuate this structure are evaluated. The first one would mimic the way we apply the displacement in the previous simulations and in the actual prototype (Figure 8-9). The second one would take advantage of the movement mechanism that the

structure has. The connectors, as previously seen, are disposed in diagonal lines which transmit the rotation to the whole structure. Taking one of these diagonals and rotating the first bar on it would possibly (at this point) actuate the entire structure. It would later be only a matter of studying how far the actuation of one of these diagonal goes and how many of this diagonals would need to be actuated depending on the size of the structure. This type of actuation would avoid the need of wrapping the entire structure.

In order to evaluate this last option some simulations were run with the same model as before and the next conditions:

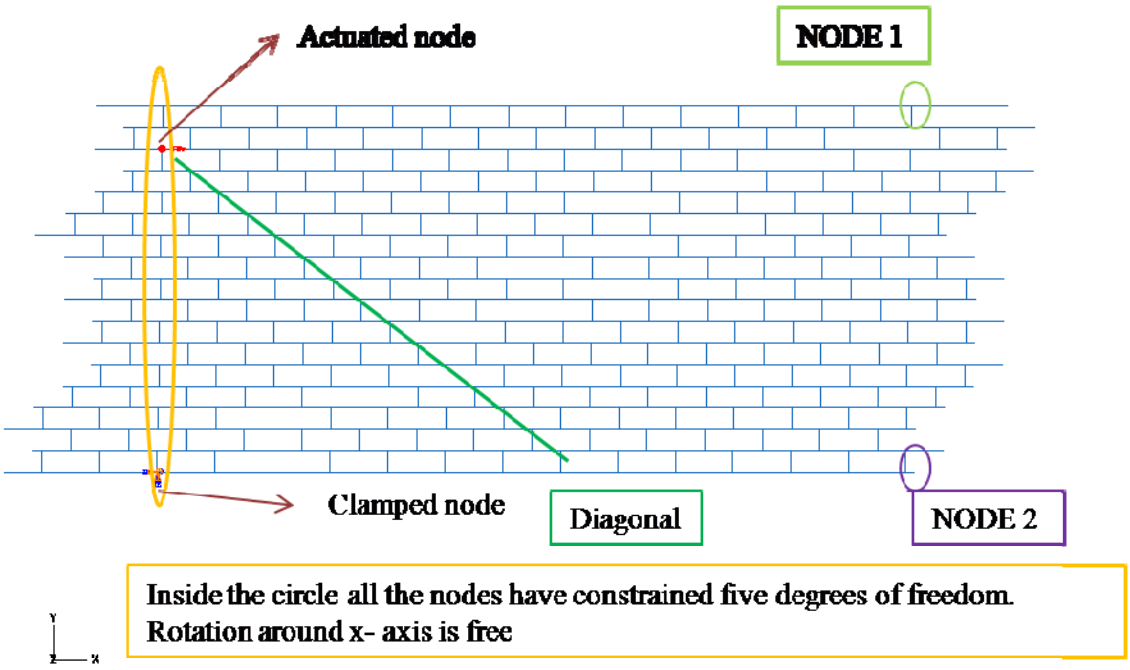

Figure 20. Boundary conditions for the simulation using the rotation property of the clamped nodes and the diagonal as the movement transmitter.

The initial applied rotation was 180º which gave convergence problems, due to the configuration of the structure, once the rotation applied was 145.8º.

When the achieved rotation was 104.7º the connectors overcome the 100 MPa yielding stress.

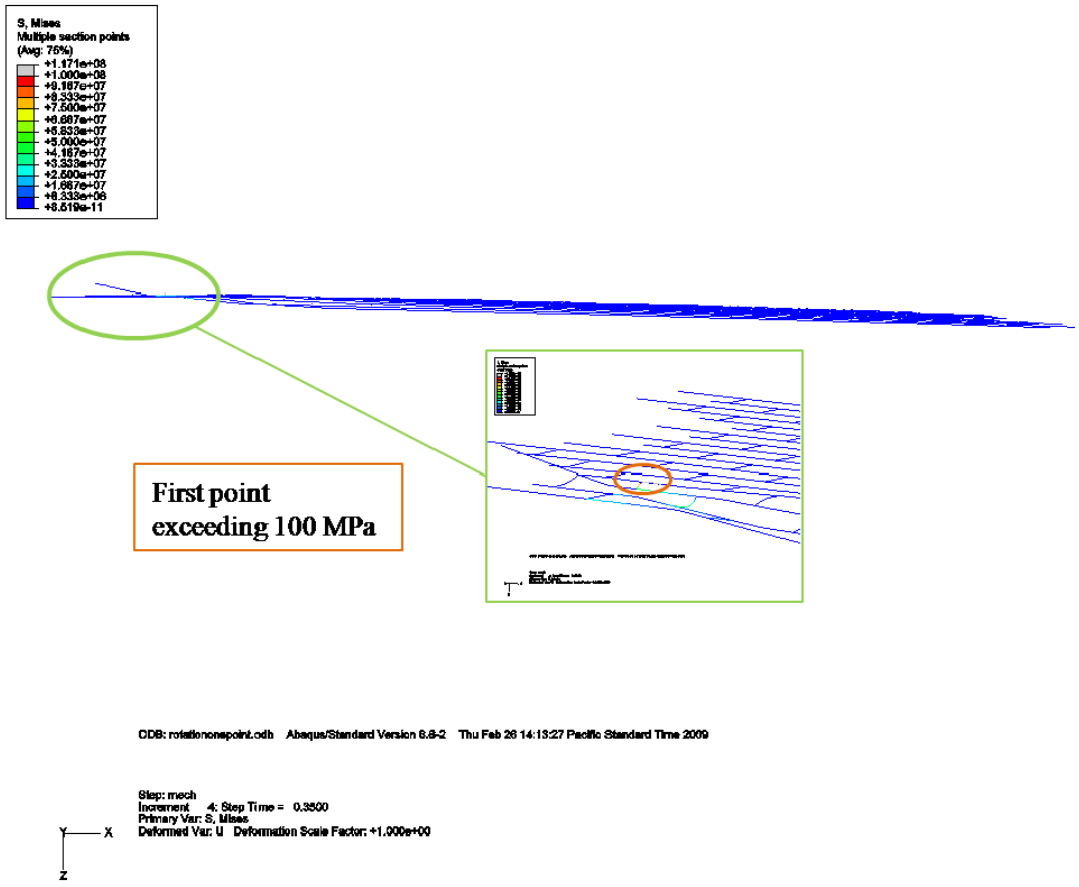

Figure 21. Failure step. The connector shown is the first point where the 100 MPa of the yielding stress are exceeded.

A last calculation to compare the single rotation to was made. A node every two connectors was actuated. All of them actuated in the same direction 180º. The rest of parameters and boundary conditions were the same as in the single rotation.

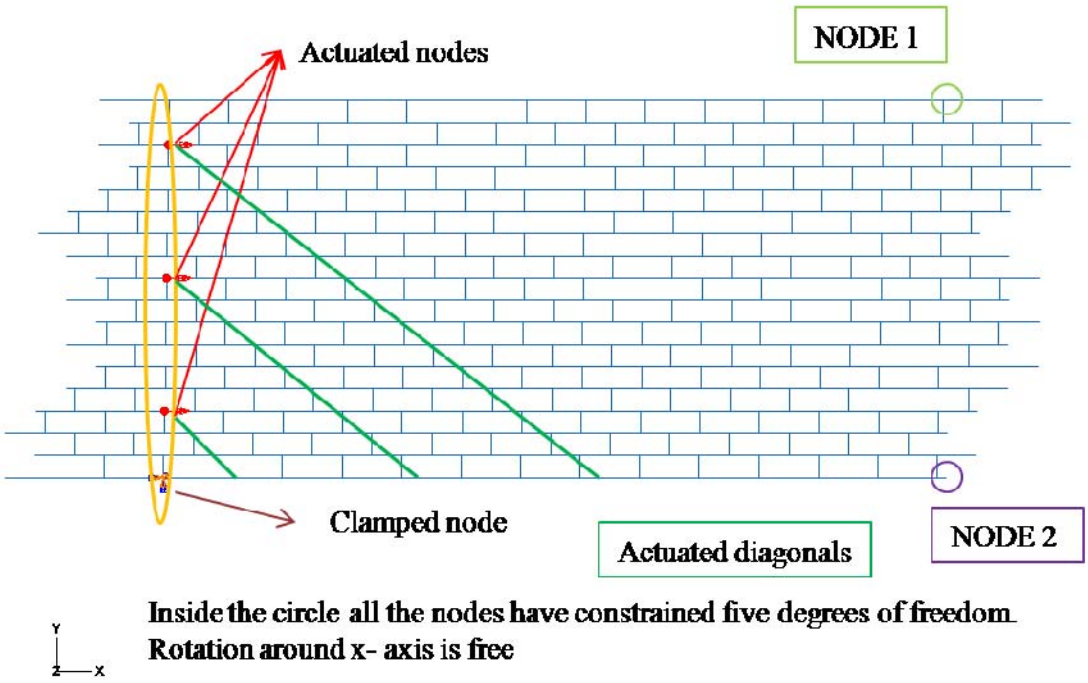

Figure 22. Boundary conditions for the simulation actuated in three nodes.

To facilitate the comparison between the two methods of actuation, the graphs shown for the previous linear deformation case will be compared with the torque needed to produce a determinate deformation in the same node (2) or angle measured as before, u_2-u_1/L. Nodes 1 and 2 are the same nodes for the two problems studied. These rotational cases give only deformations in the range of 0.001 to 0.1 m for the u_2/L and u_2-u_1/L values, the next graphs have been scaled in order to compare easily the two different cases.

The next graph represents the reaction moment produced in the clamped node/s around x axis (torque) as a function of the angle produced in the other extreme of the structure, as before, u_2-u_1/L.

For the case where we actuate three nodes, the reaction moments have been added up.

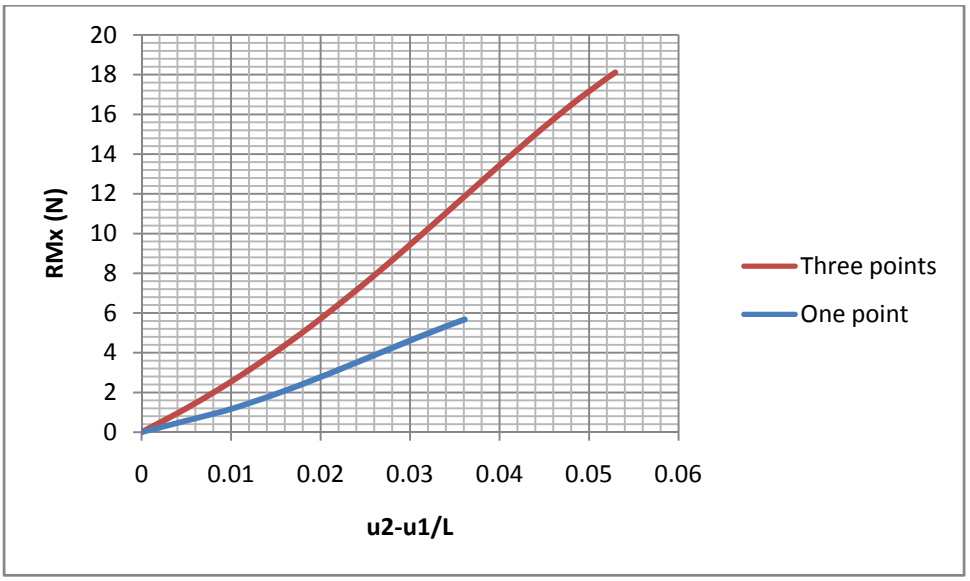

Figure 23. Torque necessary to produce a determinate angle between node 1 and 2. One point calculation stopped at 81.4% of the set up rotation. The three point calculation case stopped at 82.9% of the set up rotation.

For the three point rotation case the angle achieved is larger than the single point case but it requires a really high torque (18 N approximately).

The differences for the torque as a function of displacement in node 2 are shown in the next graph.

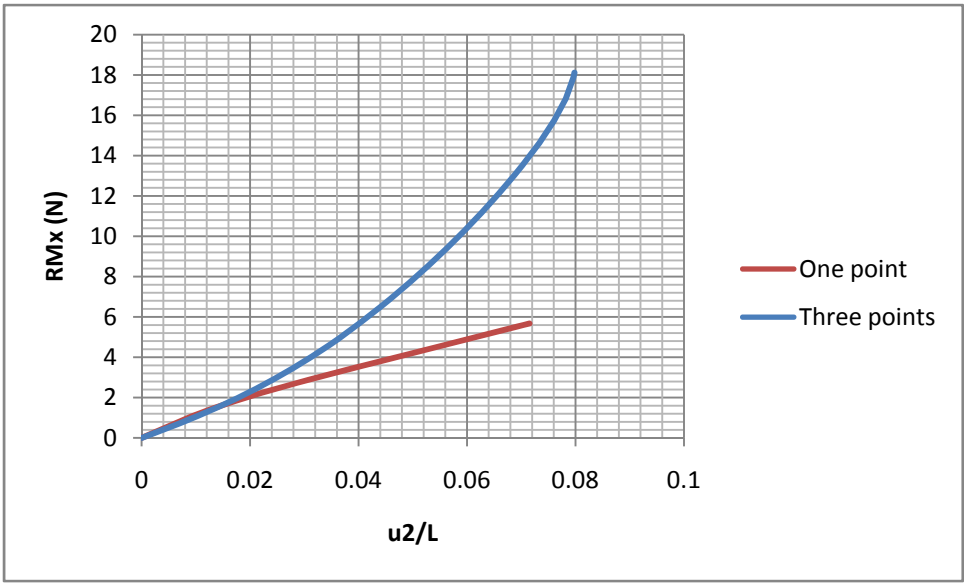

Figure 24. Torque necessary to produce a determinate displacement in node 2. One point calculation stopped at 81.4% of the set up rotation. The three point calculation case stopped at 82.9% of the set up rotation.

When the structure deflects 20 mm in –z direction, the behavior for the two studied cases diverges.

As it is inferred in the graphs shown, the second method of actuation achieves a considerable lower deflection compared with the first case studied. That added up to the difficulties on wrapping the structure in future steps makes this method not competitive with other approaches.

5. CONCLUSIONS AND FUTURE WORK

A new synthetic structure that mimics an actual deformable swimming body has been built, based on the actual morphology of oscillatory swimmers. A mechanism hidden in the structure has been shown. Such mechanism allows interesting actuation patterns with a very limited number of actuators contrasting with the presented competing concepts. A model that represents the structure has been tested through different numerical simulations based on the commercial Finite Element package ABAQUS. Different types of connectors have been studied to gain a better understanding of the kinematic behavior of the morphing plate built.

Finally, the deflections achieved are in good agreement with those achieved through different approaches (ie. Tensegrity structures) presented in this work.

Therefore, it is concluded that this work supports a novel approach for the design of a high-authority morphing structure although an extensive amount of work needs to be done in the future to study its full capabilities. Further research is suggested regarding to scaling of the structure, the actuation of the structure, actuation schemes and durability and manufacturability.

6. BIBLIOGRAPHY

[1] Schaefer J.T., Summers A.P., “Batoid Wing Skeletal Structure: Novel Morphologies, Mechanical Implications, and Phylogenetic Patterns”, Journal of Morphology 264:298-313 (2005)

[2] http://www.junglewalk.com/shop/Products/Atlantic-Manta-Ray-Poster-4636.htm

[3] Klausewitz W., “Der lokomotionsmodus der Flugelrochen *(Myliobatoidei)”*. Zool Anz 173:111-120 (1964)

[4] Heine C., “Mechanics of flapping fin locomotion in the cownose ray, *Rhinoptera bonasus* (Elasmobranchii: Myliobatidae)”. Durham, NC: Duke University (1992)

[5] Compagno L.J.V., “Endoskeleton”. In: Hamlett WC, editor. Sharks, skates, and rays: the biology of elasmobranch fishes. Baltimore: Johns Hopkins University Press. p 69-92 (1999)

[6] Liem K.F., Summers A.P., “Muscular system: gross anatomy and functional morphology of muscles”. In: Hamlett WC, editor. Sharks, skates, and rays: the biology of elasmobranch fishes. Baltimore: Johns Hopkins University Press. p 93-114 (1999)

[7] Schaefer J.T., “Modeling physical properties of joint arrays in batoid wings”. Journal of morphology, Vol. 268, issue:12, pp. 1129-1129 (2007)

[8] Rosenberger L.J., “Pectoral fin locomotion in batoid fishes: undulation versus oscillation”. J Exp Biol 204:379-394

[9] Han H.L., Lu T.J., Evans A.G., “Optimal Design of a Novel High Authority SMA Actuator”. Mechanics of Advanced Materials and Structures, 12:217-227 (2005)

[10] Sofla A.Y.N., Elzey D.M., Wadley H.N.G., “Two-way Antagonistic Shape Actuation Based on the One-way Shape Memory Effect”. Journal of Intelligent Material Systems and Structures, Vol. 19, pp. 1017-1027 (September 2008)

[11] Duerig T.W., Melton K.N., Stockel D. and Wayman, Engineering Aspects of Shape Memory Alloys, Butterworth-Heinemann Ltd, UK (1990)

[12] Lu T.J., Hutchinson J.W. Evans A.G., “Optimal Design of a Flexural Actuator”, J. Mech. Physics of Solids, vol.49, pp. 2071-2093 (2001)

[13] Elzey D.M., Sofla, A.Y. N. and Wadley H.N.G., “Shape Memory-based Structural Actuator Panel”, In: Proceedings of the SPIE –The International Society for Optical Engineering, Vol. 4698, pp. 192-200 (2002)

[14] Elzey D.M., Sofla, A.Y. N. and Wadley H.N.G., “A Shape Memory-based Multifunctional Structural Actuator Panel”, International Journal of Solid and Structures, 42:1943-1955 (2005)

[15] Elzey D.M., Sofla, A.Y. N. and Wadley H.N.G., “A Bioinspired, High Authority Actuator for Shape Morphing Structures”, In: Lagoudas, D. (ed.), Proceedings of SPIE: Smart Structures and Materials: Active Materials Behavior and Mechanics, Vol. 5053, pp. 92-100 (2003)

[16] Sofla A.Y.N., Elzey D.M., and Wadley H.N.G., “An antagonistic Flexural Unit Cell for Design of Shape Morphing Structures”, In: Proceedings of the ASME

Aerospace Division: Adaptive Materials and Systems, Aerospace Materials and Structures, pp. 261-269, Anaheim, CA.

[17] Guest S.D., Hutchinson J.W., “On the determinacy of repetitive structures”, Journal of the Mechanics and Physics of Solids 51, 393-391 (2003)

[18] Dos Santos e Lucato S. L., Wang J., Maxwell P., McMeeking R.M., Evans A.G., “Design and demonstration of a high authority shape morphing structure”, International Journal of Solids and Structures 41, 3521-3543 (2004)

[19] Hutchinson R.G., Wicks N., Evans A.G., Fleck N.A., Hutchinson J.W., “Kagome plate structures for actuation”, Int. J. Solids Struct. 40, 6969-6980 (2003)

[20] Moored K.W., Bart-Smith H., “The Analysis of Tensegrity Structures for the Design of a Morphing Wing”. Transactions of the ASME, vol.74, pp.668-676 (July, 2007)

[21] Hernandez Juan S., Mirats Tur J.M., “Tensegrity frameworks: Static analysis review”, Mechanism and Machine Theory, 43, 859-881 (2008)

[22] Moored K.W., and Bart-Smith H., “The Analysis of Tensegrity Structures for the Design of a Morphing Wing”, Proceedings of IMECE’05, Orlando, FL, November 8-12, ASME, New York

[23] Abaqus/CAE User’s Manual

[24] http://www.matweb.com/